JOURNAL OF SOLID STATE CHEMISTRY 25, 239–250 (1978)

Structural Phase Transition in Mixed Crystals $W_xMO_{1-x}O_3$

E. SALJE AND R. GEHLIG

Mineralogisches Institut, TU Hannover, D3 Hannover, Welfengarten 1, Germany

AND K. VISWANATHAN

Mineral. – Petrolog. Institut, TU Braunschweig, Gaussstrasse 29, Germany

Received October 31, 1977; in final form January 17, 1978

Crystals of $W_xMo_{1-x}O_3$ have been grown. The phase diagram shows 12 different phases. Their structures are closely related to the corresponding WO_3 phases except for $x < 0.05\%$ where an MoO_3-like structure was found. The structural parameters are given and discussed on the basis of their group theoretical sequences. Raman and infrared spectra revealed a strong dependence of the lowest energetic phonon branch (50 cm^{-1}) and the 650 cm^{-1} mode on chemical composition. Thermal soft modes were found for $W_{0.78}MO_{0.22}O_3$.

Introduction

Pure WO_3 has been widely studied for several years because of its interesting dielectric, electrochromic, and structural properties. As some of these parameters strongly depend on impurities or doping, attempts were made in the past to grow mixed crystals systematically. Two significant ways were found to produce highly conducting crystals: the reduction to WO_{3-x} (*1*) or the formation of different tungsten bronzes M_xWO_3. For electrochromic devise applications, low conducting specimens are required. To reduce the conductivity additional electron traps should be created. This seemed to be possible by replacing W by Mo in $W_xMo_{1-x}O_3$. In this system both end members reveal octahedral environments of the heavy metal atoms but different octahedral networks. The aim of this paper is to give details of the growth of the mixed crystals and to examine their structural properties. As most of the high-temperature structural phase transitions in pure WO_3 are correlated with a critical behavior of optical phonons (*2*), additional information on the phonon branches was obtained by Raman and infrared spectroscopy.

Preparation of Crystals

Tungsten trioxide powder (Merck No. 829) which had been annealed at 800°C for 3 days and molybdenum trioxide (Merck No. 401) were chosen as starting materials. Mixtures of the trioxides with chemical compositions of $WO_3/MoO_3 = 3, 2, 1, 0.5, 0.33$, and 0.2 were ground in an agate mortar and pressed to pellets. These pellets were sealed in quartz tubes (length 10 cm, diameter 1.5 cm) which were heated in a vertical furnace for 3 days. The reaction temperatures was varied from 500 to 1100°C in steps of 50°C. The temperature over the length of the tubes showed a gradient of about 100°C though the

0022-4596/78/0253-0239$02.00/0

gradient within the specimen was only about 5°C. In order to prepare single crystals of sizes up to 1 × 0.5 × 5 cm, the trioxides were heated in a horizontal furnace for 14 days. In this case the temperature gradient was 200°C over the tube length. The samples were cooled rapidly to room temperature. The chemical composition of the mixed crystals was determined with help of X-ray fluorescence. In addition the chemical composition was checked by heating the crystals to 800°C thereby allowing all the molybdenum trioxide to evaporate and then determining the loss of weight. The error in the chemical composition by this method was less ±3%.

Three different phases could be distinguished at room temperature from their morphology:

(1) Crystals with Mo content less than 25 mole% exhibit a flat pyramidal, bipyramidal, or sphenoidic habit on {112} and {111}. Pure WO_3 shows the same form when it is synthesized at temperatures below 1000°C (*3*, *4*). Optical examination revealed monoclinic or triclinic properties similar to WO_3(I) and WO_3(II) (*5*).

(2) Crystals with molybdenum contents of 25 to 70 mole% MoO_3 are needle-shaped with pseudotetragonal symmetry. The color is bright yellow or green. They are extremely fragile. These crystals are optically monoclinic.

(3) Samples with less than 3 mole% WO_3 show the same habit as pure MoO_3 but give rise to much bigger crystals. Their colors are slightly yellowish (up to 2% WO_3) or light blue (3% WO_3) with a strong pleochroism.

X-Ray Experiments and Structure Analysis[1]

The crystals have been examined by means of X-ray methods. For determination of lattice constants, a high-temperature Guinier camera employing $CuK\alpha_1$ radiation was used (*5*). Structure analysis was carried out by film methods with Weissenberg and Precession cameras. Zr-filtered Mo radiation was used. The intensities were measured with a photodensitometer.

The atomic parameters were refined using an ORFLS routine and the interatomic distances and angles were calculated with a SADIAN program.

At room temperature five different structures can be distinguished from their lattice constants. Four of them, δ, γ, ε, and μ are isostructural to WO_3(I), WO_3(II), WO_3 (−40°C), and MoO_3. For clarity, all phases of the ternary system W–Mo–O are indexed with Greek letters. In addition to these four phases a new one, ζ, appears for the mixed crystals. At higher temperatures, two unknown structures η and θ are found with monoclinic and orthorhombic symmetry and almost the same scattering intensities. By rapid cooling, the θ phase could be quenched and found in some powders at room temperature.

The lattice constants of the different phases are collected in Tables Ia, b, c. For the new structures ζ and θ, powder diffraction inten-

TABLE Ia

LATTICE CONSTANTS OF THE COMPOUND $W_{0.4}Mo_{0.6}O_3$ AT DIFFERENT TEMPERATURES

Phase present	Temp. (°C)	a (Å)	b (Å)	c (Å)	α (°)	β (°)	γ (°)	Vol.
θ	550	5.409	5.574	7.206	90.00	90.00	90.00	217.3
η	450	5.565	5.398	7.196	90.00	90.00	90.00	216.1
η	350	5.555	5.386	7.199	90.00	91.26	90.00	215.3
η	250	5.551	5.372	7.189	90.00	91.36	90.00	214.3
ζ	25	7.433	7.420	7.610	90.00	91.39	90.00	419.6
θ (metastable)	25	5.331	5.519	7.189	90.00	90.00	90.00	211.5

[1] See note added in proof.

TABLE Ib

LATTICE CONSTANTS OF "ζ" PHASE

Composition	a	b	c	α	β	γ	Vol.
$W_{0.26}Mo_{0.74}O_3$	7.433	7.420	7.610	90.00	91.39	90.00	419.6
$W_{0.28}Mo_{0.72}O_3$	7.435	7.425	7.614	90.00	91.39	90.00	420.15
$W_{0.42}Mo_{0.58}O_3$	7.439	7.422	7.610	90.00	91.29	90.00	420.08
$W_{0.53}Mo_{0.47}O_3$	7.438	7.425	7.607	90.00	91.28	90.00	420.02
$W_{0.62}Mo_{0.38}O_3$	7.446	7.420	7.611	90.00	91.22	90.00	420.45
$W_{0.67}Mo_{0.33}O_3$	7.440	7.419	7.608	90.00	91.30	90.00	419.8
$W_{0.71}Mo_{0.29}O_3$	7.446	7.424	7.613	90.00	91.24	90.00	420.7

TABLE Ic

LATTICE CONSTANTS OF DOPED MoO_3 AT DIFFERENT TEMPERATURES

T (°C)	a	b	c	Vol.	Sp. No.
−75	3.960	13.794	3.699	202.09	39/1
−70	3.959	13.796	3.702	202.22	41/1
R.T. (20)	3.959	13.864	3.697	202.98	41/1
R.T. (20)	3.961	13.855	3.698	202.96	39/1
40	3.961	13.855	3.699	203.04	41/1
103	3.963	13.879	3.698	203.4	41/1
175	3.965	13.931	3.694	204.0	39/1
175	3.965	13.933	3.694	204.1	41/1
250	3.966	13.990	3.695	205.03	41/1
250	3.967	14.027	3.693	205.48	41/1
270	3.971	14.034	3.693	205.79	39/1
293	3.969	14.062	3.692	206.09	41/1
360	3.972	14.110	3.692	206.92	41/1
370	3.973	14.115	3.689	206.88	39/1
410	3.976	14.153	3.690	207.63	41/1
450	3.979	14.195	3.686	208.21	39/1
490	3.978	14.202	3.689	208.42	41/1

TABLE II

POWDER DATA OF $W_{0.4}Mo_{0.6}O_3$ (sp·gr = $Cmc2_1$) (θ PHASE) OBTAINED AT ROOM TEMPERATURE $Z = 4$.

h	k	l	I_0	d_o	d_c
1	1	0	100	3.840	3.834
0	0	2	66	3.596	3.594
1	1	1	49	3.381	3.383
0	2	0	6	2.759	2.759
2	0	0	23	2.666	2.665
1	1	2	78	2.626	2.622
0	2	1	32	2.578	2.576
0	2	2	8	2.187	2.188
2	0	2	11	2.141	2.141
1	1	3	21	2.026	2.032
2	2	0	22	1.917	1.917
2	2	1	36	1.852	1.852
0	2	3	20	1.809	1.809
0	0	4	27	1.797	1.797
2	2	2		1.690	1.691
3	1	0	20	1.690	1.691
1	3	1		1.690	1.690
3	1	1	7	1.646	1.646
1	1	4	38	1.627	1.627
3	1	2	23	1.530	1.530
0	2	4	7	1.506	1.506
2	2	3	21	1.497	1.497
2	0	4	17	1.490	1.490

sities and diffraction angles are listed in Tables II and III. For both forms, structure analysis work was carried out.

The ζ structure was solved using a crystal of the dimension 0.1 × 0.15 × 0.03 mm and a chemical composition of $W_{0.7}Mo_{0.3}O_3$ as determined from the surrounding bulk material during crystal growth. The crystal was twinned with the twinning plane (100). Therefore some reflections with low 2θ scattering angles could not be separated accurately and were not used for the structure analysis. From the systematic extinctions, the space group $P2_1/n$ was assumed. Using this symmetry, the structure was refined on the basis of 300 independent reflections. As starting parameters, the atomic positions of the γ phase (δ) were chosen. The refinement converged rapidly to an R value of 8.9%. The final atomic positions and interatomic distances are listed in Tables IV and V. A plot of the structure is shown in Fig. 1.

TABLE III

POWDER DATA OF $W_{0.53}Mo_{0.47}O_3$ (ζ PHASE) AT ROOM TEMPERATURE

			I (Obs)						I (Obs)		
h	k	l		D (Obs)	D (Calc)	h	k	l		D (Obs)	D (Calc)
0	0	2	55	3.801	3.802	−3	1	1	3	2.260	2.259
2	0	0	100	3.721	3.718	−2	2	2	25	2.177	2.177
0	2	0		3.721	3.712	2	2	2	26	2.146	2.145
1	2	0	16	3.317	3.321	3	2	0	11	2.061	2.061
−1	1	2	32	3.102	3.103	2	1	−3	3	2.034	2.035
2	1	−1	20	3.068	3.068	3	1	−2	23	2.019	2.018
1	1	2	28	3.054	3.057	1	3	−2	22	2.003	2.004
2	1	1	14	3.024	3.024	1	3	2	22	1.991	1.991
2	0	−2	18	2.688	2.688	3	1	2	21	1.982	1.981
0	2	2	30	2.657	2.656	0	0	4	16	1.902	1.901
2	2	0	60	2.627	2.627	4	0	0	24	1.859	1.859
2	0	2		2.627	2.629	0	4	0	28	1.855	1.856
−1	2	2	11	2.516	2.514	1	1	4	35	1.779	1.778
1	2	2	9	2.488	2.489	4	1	−1	24	1.762	1.763
1	0	3	5	2.381	2.383	4	1	1	23	1.746	1.746

TABLE IV

ATOMIC PARAMETERS OF ζ PHASE

	x	y	z
W_1	0.2724	0.0161	0.2865
W_2	0.2271	0.0238	0.7821
O_{x1}	0.0032	0.0393	0.2097
O_{x2}	−0.0058	0.4587	0.2109
O_{y1}	0.2863	0.2573	0.2925
O_{y2}	0.2030	0.2539	0.7227
O_{z1}	0.2884	0.0441	0.0037
O_{z2}	0.2833	0.4673	−0.0033

TABLE V

INTERATOMIC DISTANCES AND ANGLES FOR ζ PHASE[a]

(a) W_1 octahedron (Å)		(b) W_2 octahedron (Å)	
W_1–O_{x1}	2.083	W_2–O_{x1}	1.782
W_1–$O_{x2'}$	1.791	W_2–$O_{x2''}$	2.078
W_1–O_{y1}	1.795	W_2–O_{y2}	1.776
W_1–$O_{y1'}$	2.058	W_2–$O_{y2'}$	2.072
W_1–O_{z1}	2.169	W_2–O_{z1}	1.745
W_1–O_{z2}	1.750	W_2–$O_{z2'}$	2.164
O–W_1–O angles vary from 77.76 to 101.4°		O–W_2–O angles vary from 76.64 to 102.7°	

[a] Primed and unprimed atoms are related by screw axes.

The structure of the ζ phase is similar to that of monoclinic WO_3 (γ). The distribution of the heavy metal atoms on the symmetry independent positions is almost random. Further attempts to refine the structure under lower symmetry ($P2_1$ and Pn) revealed no significant deviations from the random distribution. Geometrically, the W and Mo atoms are off centered from their octahedra midpoints,

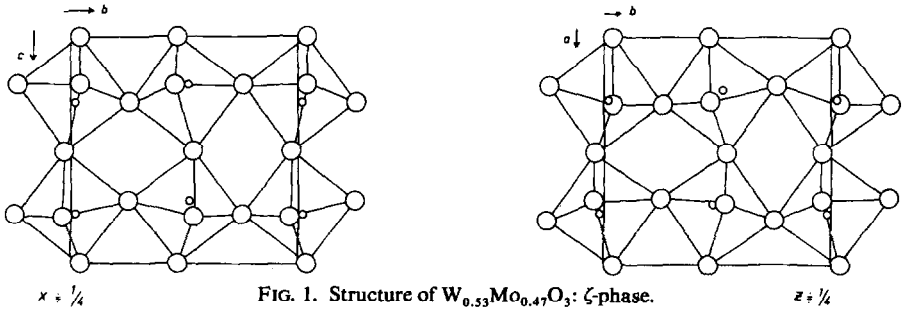

FIG. 1. Structure of $W_{0.53}Mo_{0.47}O_3$: ζ-phase.

forming zig-zag chains along b and a, in contrast to the γ phase. The oxygen octahedra are tilted around the c axis and around the a axis.

The structure of the θ phase could be determined only by powder methods. It was concluded from the systematic extinctions, that the space group must be *Cmcm*, or *C2cm*, or $Cmc2_1$. In all these symmetries, the W and Mo positions must be distributed on four symmetry equivalent positions statistically. As θ is a high temperature phase of a piezoelectric one only the acentric subgroups *C2cm* abd $Cmc2_1$ are considered for refinements. As the superstructure along the c axis is strong, as indicated by intense reflections like 111, 021, 113, and 221, a considerable deviation of the (W, Mo) positions from the octahedra midpoints was concluded. This knowledge fixed the heavy metal positions on $(0, y, \frac{1}{4})$ with only one free parameter. The starting parameters of oxygen were approximately determined from packing considerations. The structure was then refined with an ORFLS program to an R value of 5.9%. Further refinements under the subgroup symmetries gave the same parameters for the heavy metals and oxygen in the $z = \frac{1}{4}$ and $z = \frac{3}{4}$ layers within experimental error. The remaining oxygen positions between the layers could

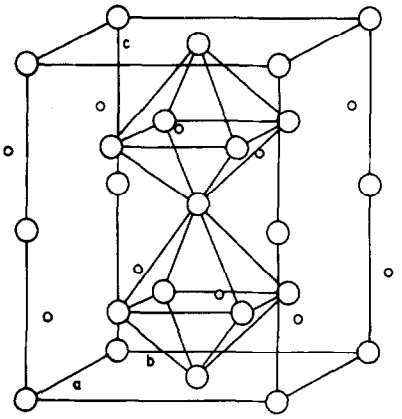

FIG. 2. Structure of $W_{0.4}M_{0.6}O_3$: θ-phase.

TABLE VI

DATA CONCERNING THE STRUCTURE OF $W_{0.4}Mo_{0.6}O_3$ (θ PHASE)

(a) Observed and calculated structure factors

h	k	l	F_o	F_c
1	1	0	200.4	216.8
0	0	2	238.2	238.2
1	1	1	106.6	106.3
0	2	0	81.1	84.3
0	2	1	142.2	155.4
2	2	1	133.8	140.7
0	2	3	142.6	137.7
2	0	0	169.7	176.9
1	1	2	156.7	152.3
3	1	1	62.2	55.9
1	1	4	151.6	157.6
3	1	2	124.4	127.0
0	2	4	95.9	77.5
2	2	3	118.5	127.9
2	0	4	152.4	146.7
2	2	0	145.7	147.8
1	1	3	96.1	90.0
0	0	4	239.1	216.7
R = 0.053				

(b) Atomic parameters (space group $Cmc2_1$)

	x	y	z	B
W =	0.0	0.0751	0.250	0.5
O(1) =	0.0	0.064	−0.005	
O(2) =	0.216	0.254	0.269	1.0

(c) Interatomic distances

W–O(1) = 1.834; W–O(1)[a] = 1.921 Å
W–O(2) = 1.522
W–O(2′) = 2.336[b]

[a] Atoms related by c-glide planes.
[b] Primed and unprimed atoms are related by C-centering.

not be localized beyond doubt in these space groups. The atomic positions are listed in Table IV; the structure is shown in Fig. 2.

The structure of the θ phase can be described as ReO_3-like with systematic antiferrodistortive displacements of the heavy metal atoms perpendicular to the c axis. This deformation type is quite similar to that of the low-temperature phase of WO_3 (*7*).

Phase Diagram

Crystals with Mo content less than 25 mole% always show X-ray diffraction patterns like WO_3(I) and WO_3(II). Similar to pure WO_3, the bigger single crystals are mostly triclinic and transform to monoclinic symmetry above room temperature. The monoclinic phase is called γ and the triclinic one δ. For Mo content between 25 and 70 mole%, the ζ phase was found. If these crystals are ground to powder, a further phase similar to the low-temperature phase of WO_3 (*7*) is seen in the powder diagram. This phase is called ε. The same effect was often found for crystals of the γ and δ phase. Hence it is assumed that the ε phase exists in a metastable state even for high Mo contents. On heating these samples, the ε phase disappears before the γ or ζ phase transforms to their corresponding high-temperature phase.

Only crystals with low W contents (less 5 mole%) exhibit an MoO_3 like structure (μ). The lattice constants of the different phases are given in the Tables I to III.

At 150°C the δ phase transforms to the γ phase. On further heating, the γ phase disappears in a second-order transformation to the β phase, corresponding to the orthorhombic form of WO_3. The highest symmetry was found above ca. 800°C in the tetragonal α phase.

The ζ phase shows two different phase transformations depending on the chemical composition. Crystals with lower Mo content (<50%) transform to the phase γ', which has the same diffraction pattern as γ. Both phases can be distinguished by their piezoelectric effect: the γ phase is centric according to the space group $P2_1/n$. Although the γ' phase shows the same systematic extinctions even for long exposure times, this phase is slightly piezoelectric. This effect may be due to W–Mo ordering properties but is unlikely to induce geometrical differences between both structures. From group theory it is expected that the same holds for the additional high-temperature phases β' and α'. Piezoelectrical measurements are not reliable at these temperatures because of the high electrical conductivity of the samples.

Crystals with >50% Mo content, show a phase transition to the η phase and at higher temperatures to θ. All of these phases, ζ, η, δ, and θ, are slightly piezoelectric without visible deviations from their diffraction symmetry in the X-ray experiment. The true space groups are therefore assumed to be subgroups of their diffraction space groups. The η–θ transformation is second order with the monoclinic angle as the order parameter. The upper temperature of the ζ field is given by

$$T_c = 25 + 310x(°C) \quad \text{for} \quad W_xMo_{1-x}O_3.$$

Hence the approximate chemical composition can be determined from the corresponding transformation temperature. The resulting phase diagram is given in Fig. 3.

To confirm the transformation temperatures, DTA measurements were performed. In agreement with Tanisaki (*8*) and Salje and Viswanathan (*5*), the transformations ε–δ and β–α are first order. For $W_{0.33}Mo_{0.67}O_3$, $W_{0.57}Mo_{0.47}O_3$ and $W_{0.75}Mo_{0.27}O_3$ exothermic peaks are found at the ζ–γ' and ζ–η phase boundaries and none for the γ'–β' and η–θ second-order transformations. The transition enthalpies (ΔH) and entropies (ΔS) are:

$W_{0.33}Mo_{0.67}O_3$ (ζ–η): $\Delta H = 176$ J mole^{-1}, $\Delta S = 0.34$ J k^{-1} mole^{-1};

$W_{0.73}Mo_{0.27}O_3$ (ζ–γ'): $\Delta H = 213$ J mole^{-1}, $\Delta S = 0.51$ J k^{-1} mole^{-1}.

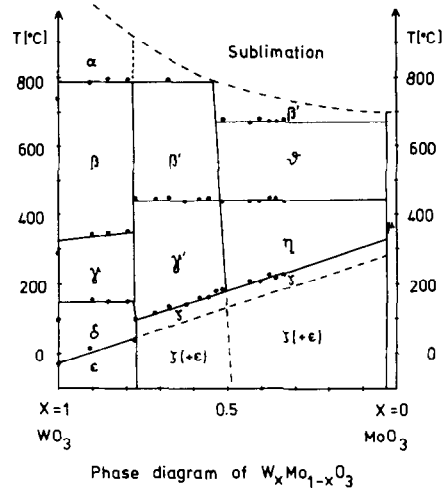

FIG. 3. Phase diagram of $W_xMo_{1-x}O_3$.

Group Theoretical Sequencies of $W_xMo_{1-x}O_3$ Structures

All structures of the system WO_3–MoO_3, except nearly pure MoO_3, reveal perovskite-like arrangements of corner-sharing octahedral networks. The differences follow from characteristic deformations of these networks, namely, the tilts of the oxygen octahedra and the offcentering of the heavy metal atoms in these octahedra (*9*). Additional symmetry reduction is probably caused by partial ordering of W–Mo. The mechanism of transformation between the different space groups and the possible order parameter symmetries can be developed from this group theoretical considerations of these structures. To derive the group sequences, subgroups—klassengleich and translationsgleich —of the different phases have to be examined (*10*). The space groups of the phases β (e.g., orthorhombic WO_3) *Pmnb* and γ (e.g., monoclinic WO_3) $P2_1/n$ are correlated by the zellengleich relation (*10*). Therefore a second-order phase transformation with a critical Γ point of the Brillouin zone is presumable. In contrast to this behavior, the transition α–β is described by a two-step sequence of space groups (α-*P4/nmm*–β-*Pmnb*). An intermediate phase was not found. As no order parameter exists in this Landau scheme (over all the Brillouin zone) the phase transformation is first order.

In Fig. 4 the group theoretical sequences are given for the different phases. The scheme can be divided into three branches of sequences. The first branch, valid for W-rich compounds, contains the phase α–β–γ–δ. Although the transformation δ–ε really takes place at low temperatures, both phases are not symmetry related and the transformation is clearly first order. The ζ phase with space group *Pn* as possible subgroup of $P2_1/n$ is theoretically part of the first branch, but was never found for W-rich compounds. The transformation from the

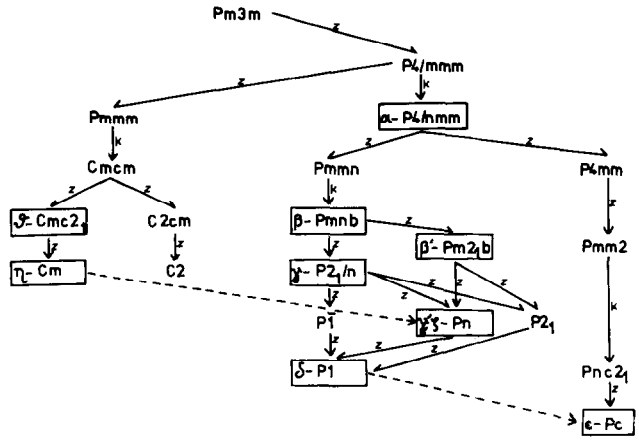

FIG. 4. Group theoretical sequences of the $W_xMo_{1-x}O_3$ structures Z: Zellengleich, k: klassengleich/translationsgleich. Parallel branches could not be distinguished from X-ray systematic extinctions.

centric γ phase to the piezoelectric δ structure is first order too. The ζ phase exists only for Mo-richer compounds with first-order transition to η. At lower temperatures a $P1$ phase is possible but was not found yet.

The second branch α–ε contains only two phases which were obtained experimentally. The space groups Pc (ε) and Pn, which may apply for ζ correspond to different orientations of the unit cells in the octahedra network.

The third branch is valid for the Mo-rich phases θ and η. X-ray experiments show only the supergroup symmetry $Cmcm$ for θ. The accentric subgroups are $Cmc2_1$ and $C2cm$ and both sequences are given in the scheme. From Fig. 4 the different transformations are grouped into three types.

(1) Second-order transformations without change of the unit cell, e.g., β–γ, η–θ;

(2) First-order transformations within the same branch of the scheme, e.g. δ–γ, α–β; The character of the transformation is stepwise, but the structures of the two phases are very closely related.

(3) First-order transformations between two different branches of the scheme, e.g., η–ζ,

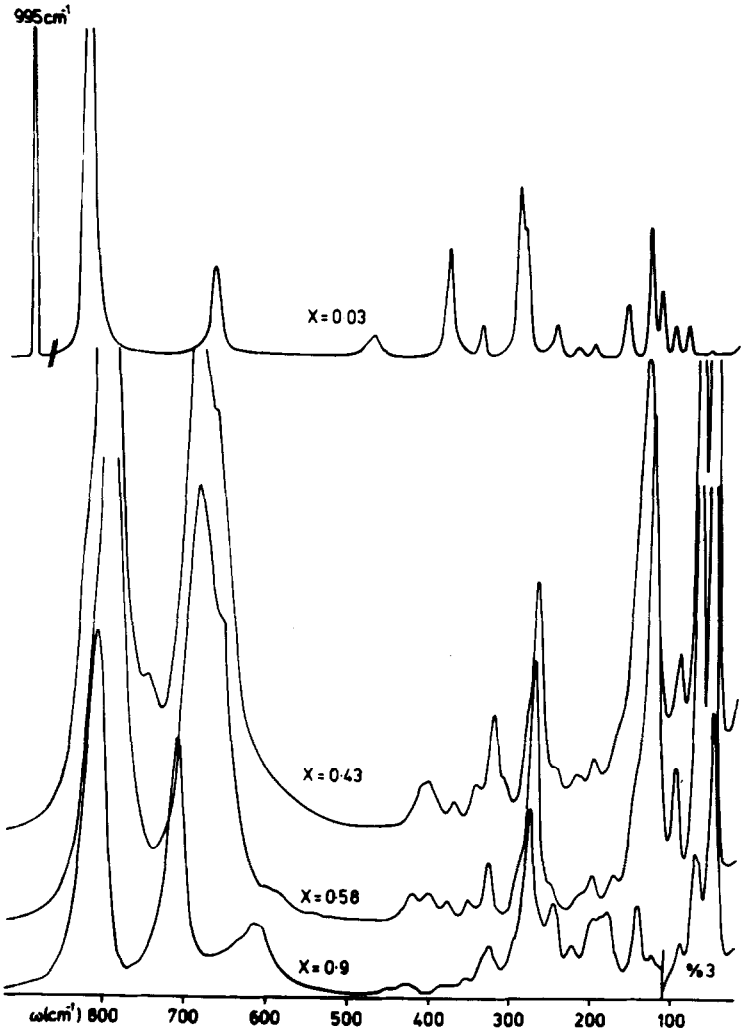

FIG. 5. Raman spectra of mixed crystals.

δ–ε; The character of the transformation is clearly first order and topotactical in nature.

A further possibility is the interchange of the whole classification scheme, which would appear during a transformation between WO_3- and MoO_3-like structures. Such a transformation is similar to renucleation and need not be topotactic. This extreme transition does not take place in the $W_xMo_{1-x}O_3$ system so far as is known.

Phonon Spectroscopy

The optical phonon lines have been measured by using infrared and Raman spectroscopy. The experimental techniques have been described before (*11*, *12*). At room temperature, the phases γ, δ, ζ, and μ could be distinguished from their phonon spectra. The Raman scattering of the low-temperature ε phase, monoclinic WO_3 (γ), and the triclinic form (δ) are identical as in (*11*). The spectra of the new phases δ, $\zeta_{x=0.58}$, $\zeta_{x=0.43}$, and μ are given in Fig. 5. The infrared absorption spectra of the powdered samples are compared in Fig. 6. For pure WO_3(II), infrared reflection measurements have been performed for single crystals. The unpolarized spectrum is given in Fig. 7, showing an infrared cutoff frequency near 1010 cm^{-1}, corresponding to the highest frequency longitudinal optical phonon. This value is near the highest TO mode in the powder absorption spectrum (920 cm^{-1}).

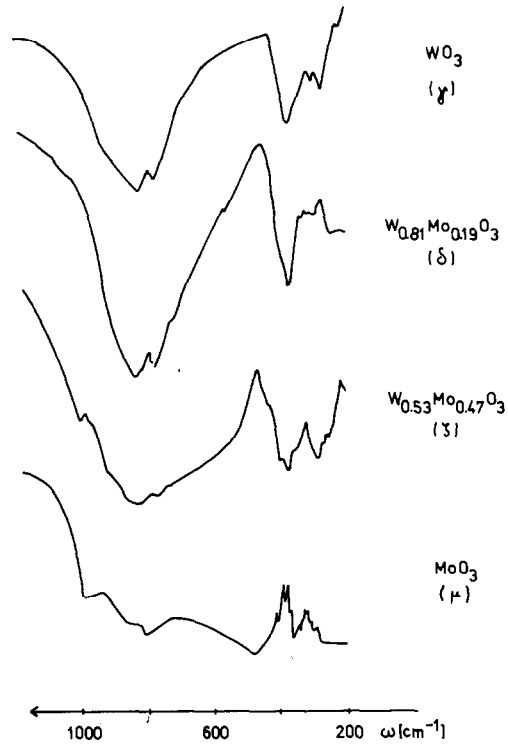

FIG. 6. Infrared in dependence on the chemical composition.

Therefore the LO–TO splitting of WO_3(II) and the related mixed crystals are very small. Considering the high Coulomb coefficient of these Slater modes (*13*) of 22 e^2/V, the effective ionic charges must be small for the heavy metal atoms, in accordance with first calculations (*9*).

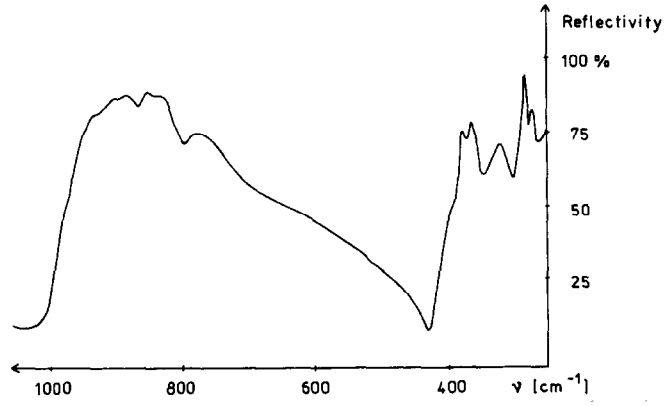

FIG. 7. Infrared spectrum of WO_3(II).

TABLE VII

PHONON FREQUENCIES OF MIXED CRYSTALS[a]

$:WO_3:Mo(I)$		$:W_{0.9}Mo_{0.1}O_3$		$:W_{0.43}Mo_{0.57}O_3$		$:MoO_3:W$	
R	ir	R	ir	R	ir	R	ir
30	230	47	230	57	245*	55*	285
66	285	70	285	73	265	83	377
73	310	84	310	100	287	100	570
93	335	98*	335	137	336	117	821
133	370	122*	370	153	369	129	870
168*	665	139	665	170*	388	158	996
190*	765	180*	765	204	435	195*	
209*	825	191*	825	224	665	200	
224*	920	196*	920	252*	765	219	
275		217*		274*	825	245	
297		221		287*	998	285	
330		246		317*		290	
352		262		328		338	
380*		276		350		367*	
402*		293*		376		378	
418*		325		409		473	
438*		335*		412*		478*	
453*		352*		672		666	
718		373*		694		820	
808		418*		755*		995	
		421*		806			
		433*					
		452*					
		615					
		711					
		813					

[a] *: weak lines, R: Raman, ir: infrared adsorption.

The phonon frequencies are listed in Table VII for the different phases. The number of the phonon branches is high in all phases. This is due to the low symmetries and big unit cells of these structures. The irreducible representations have been calculated from group theory and can be seen together with the correlation scheme between the different phases in Fig. 8. Here 45 optical modes are expected in the phases ε, η, and θ; 93 for β, γ, δ, and ζ.

The dependence of the Raman active phonon frequencies on chemical composition at room temperature is shown in Fig. 9. The three phases γ, δ, and ζ can easily be distinguished from the high energy part of the spectrum alone. The monoclinic phase exhibits only two Raman-active modes near 800 and 720 cm^{-1}, whereas the triclinic δ form shows a third signal at 612 cm^{-1}. This effect is the same for the transformation $WO_3(I)$–$WO_3(II)$ as well as for γ–δ. The mixed crystals of the ζ phase show a significant split of the 680 cm^{-1} line and additional scattering signals for $x < 0.4$. In the different phases, the dependence on the chemical composition is relatively small. No especially pronounced soft mode behavior was found. The lowest frequency phonon decreases with increasing W content stepwise in the order ζ–δ–γ. Hence all these transformations are clearly first order. In ReO_3-type structures, the lowest energy mode is mainly due to torsional effects of the oxygen octahedra. The phonons concerned with the vibrations of the octahedra midpoints, the Slater mode and its orthogonal stretching

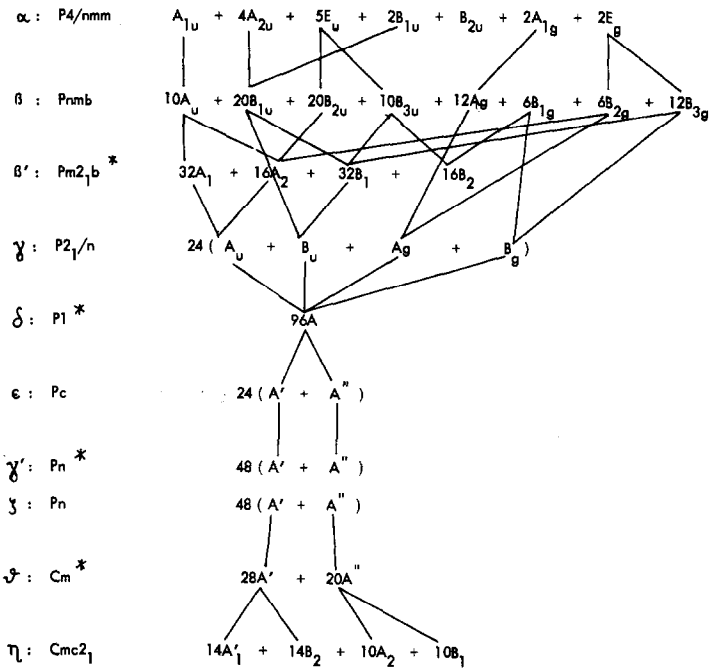

FIG 8. Correlation scheme of irreducible representations. Structures marked by an asterisk are not yet solved.

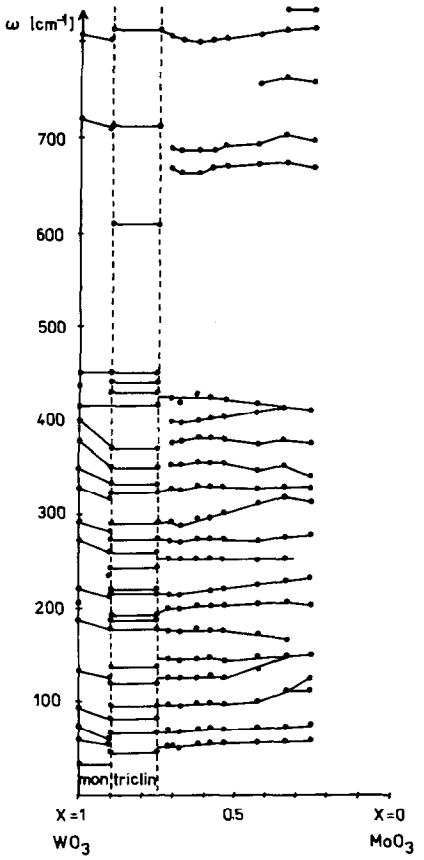

FIG. 9. Dependence of Raman lines on chemical composition at room temperature.

mode, are expected at higher frequencies, such as 700 and 300 cm^{-1}. Hence the energy levels of the octahedra torsions are lowest in the γ phase, increase to δ, and have a maximum in ζ. Structurally, the γ phase is characterized by octahedra tilts around two tilt axes and off-centering of W in one direction. In the δ phase, a further tilt in the third direction takes place, with almost the same off-centering of W. In ζ two large tilt angles occur, but antiferrodistortive deviations of the heavy metals from the octahedra midpoints occur in two directions. Hence the octahedra are heavily distorted and further tilts are not possible even at lower temperatures. With increasing temperature, the tilts become small or even vanishes in θ resembling the low-temperature ε structure, where no tilt angle was found (*7*, *14*). In this way, the γ–δ transformation is described by the spontaneous condensation of a torsional mode around the b axis, giving rise to a static tilt deformation of the octahedra network in δ.

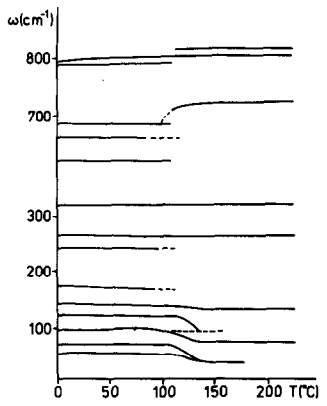

FIG. 10. Dependence of Raman scattering frequencies on temperature for $W_{0.78}Mo_{0.22}O_3$.

The fundamental change of the phonon distribution at the ζ–δ' transformation point can be seen in Fig. 10. Here the thermal dependence of the scattering frequencies for a $W_{0.78}Mo_{0.22}O_3$ crystal is shown. Below the phase transition at 110°C, the modes at 50 and 95 cm^{-1} exhibit a critical slowing down. At the transition point, most of the lines are spontaneously changed or disappear in the high-temperature form. Only the modes at 120, 280, and 320 cm^{-1} are comparably less altered. The difference of (W, Mo)–O force constants in both phases is clearly brought out by the change of the highest frequency modes, which are much stronger than during the γ–δ transformation. The 800 cm^{-1} mode is split in the γ' phase, but not in γ, which may be due to partial ordering of W–Mo.

Note Added in Proof

In the meantime new intensity data have been collected for the ζ-phase with a STOE-4-circle diffractometer using an untwinned crystal. The final structural parameters have been refined on the basis of 1520 symmetry independent reflections and are listed in Tables IV and V. The R value decreased to 4.8%. A table of observed and calculated F values is available from authors on request.

Acknowledgment

We are indebted to Dr. R. J. D. Tilley (Bradford) for helpful discussions. E.S. and K.V. are grateful to the DFG for financial support.

References

1. J. M. BERAK AND M. J. SIENKO, *J. Solid State Chem.* **2**, 109 (1970).
2. E. SALJE, *Acta Crystallogr. B* **33**, 574 (1977).
3. F. A. SCHROEDER AND H. FELSER, *Z. Kristallogr.* **135**, 391 (1972).
4. W. KLEBER, M. HOEHNERT, AND R. MUELLER, *Z. Anorg. Allgem. Chem.* **346**, 113 (1966).
5. E. SALJE AND K. VISWANATHAN, *Acta Crystallogr. A* **31**, 356 (1975).
6. B. O. LOOPSTRA AND P. RIETVELD, *Acta Crystallogr.* **25**, 1420 (1966).
7. E. SALJE, *Ferroelectrics* **12**, 215 (1976).
8. S. TANISAKI, *J. Phys. Soc. Japan* **15**, 566 (1960).
9. E. SALJE, *Acta Crystallogr. A* **32**, 233 (1976).
10. L. L. BOYLE AND J. E. LAWRENSON, *Acta Crystallogr. A* **28**, 485 (1972).
11. E. SALJE, *Acta Crystallogr. A* **31**, 360 (1975).
12. E. SALJE AND K. IISHI, *Acta Crystallogr. A* **33**, 399 (1977).
13. R. A. COWLEY, *Phys. Rev.* **134**, 981 (1964).
14. R. GAZINELLI AND O. F. SCHIRMER, to be published.